Evolution of Microstructure during the Thermal Activation of Copper(II) and Chromium(III) Doubly Promoted Tin(IV) Oxide Catalysts: An FT-IR, XRD, TEM, XANES/EXAFS, and XPS Study

Philip G. Harrison,* Nicholas C. Lloyd, Wayne Daniell, Ian K. Ball, Craig Bailey, and Wan Azelee[†]

School of Chemistry, University of Nottingham, University Park, Nottingham NG7 2RD, U.K.

Received July 4, 2000

The nature of the chemical transformations occurring during the thermal activation of chromium(III) and copper(II) doubly promoted tin(IV) oxide catalysts of three stoichiometries (Sn:Cr:Cu atom ratios 1:0.30:0.34, 1:0.30:0.13, and 1:0.13:0.27) have been investigated by a combination of FT-IR, powder X-ray diffraction, transmission electron microscopy, extended X-ray absorption fine structure and near edge structure, and X-ray photoelectron spectroscopy. The freshly prepared gel catalyst materials comprise small (ca. 1−2 nm) particles. Calcination results in a progressive increase in the size of the tin(IV) oxide particles, only slowly initially (ca. ×2 by 673 K, ca. ×10 by 873 K), but sintering to very large particles occurs at higher temperatures. No incorporation of chromium or copper into the tin(IV) oxide lattice occurs even at high temperature. Interaction of the two promoter metals at calcination temperatures of 573 K leads to the formation of copper(II) chromate(VI), $CuCrO_4$. At temperatures ≥873 K the material with a Cu:Cr ratio of 1 comprises crystalline tin(IV) oxide and copper(II) chromite(III), $CuCr_2O_4$, only. $CuCr_2O_4$ is also formed in both the copper-rich and the chromium-rich materials, but in addition in these materials crystalline CuO and Cr_2O_3, respectively, are formed. Calcination of the copper-rich material at 1273 K results in a further tranformation to copper(I) chromite(III), $Cu_2Cr_2O_4$.

Introduction

Promoted tin oxide catalyst materials, in particularly by copper(II), have been known for a long time to have good activity toward the CO/O_2 and CO/NO reactions.[1−7] Data from our laboratory[8] have demonstrated that Cr/SnO_2 and $Cu/Cr/SnO_2$ catalysts exhibit activity which is comparable to conventional noble metal catalysts. These data show that the performance of these catalysts is similar to the $Pt/Rh/Al_2O_3$ catalyst for the oxidation of CO and hydrocarbons. Activity comparable to that of noble metal catalysts has also been observed by others for alumina-supported copper and chromium,[9,10] while Cu/Cr materials have been studied extensively as catalysts for the oxidation of CO,[11−26] hydrocarbons,[27−30] sulfurated and chlorinated hydrocarbons,[31,32] and alcohols and aldehydes,[33,34] as well as for NO reduction.[35−37]

Despite this quite large effort devoted to the study of Cu/Cr catalysts, the nature and constitution as well as the role of the constituents does not appear to be well

[†] Present address: Department of Chemistry, Faculty of Science, University Technology Malaysia, Skudai, Locked Beg 791, 80990 Johor Bahru, Malaysia.

(1) Fuller, M. J.; Warwick, M. E. *J. Catal.* **1973**, *29*, 441.
(2) Fuller, M. J.; Warwick, M. E. *J. Catal.* **1974**, *34*, 445.
(3) Bond, G. C.; Molloy, L. R.; Fuller, M. J. *J. Chem. Soc., Chem. Commun.* **1975**, 796.
(4) Croft, G.; Fuller, M. J. *Nature* **1977**, *269*, 585.
(5) Fuller, M. J.; Warwick, M. E. *J. Catal.* **1976**, *42*, 418.
(6) Fuller, M. J.; Warwick, M. E. *Chem. Ind. (London)* **1976**, 787.
(7) Solymosi, F.; Kiss, J. *J. Catal.* **1978**, *54*, 42.
(8) Harrison, P. G.; Harris, P. J. U.S. Patent 4,908,192, 1990; U.S. Patent 5,051,393, 1991.
(9) Barnes G. J. *Adv. Chem. Ser.* **1975**, *No.143*, 72.
(10) Stegenga, S.; Dekker: N.; Kapteijn, F.; Moulijn, J. A. In *Catalysis and Automobile Pollution Control II*; Crucq, A., Ed.; Elsevier: Amsterdam, 1991; p 353.
(11) Hertl, W.; Farrauto, R. J. *J. Catal.* **1973**, *29*, 352.
(12) Farrauto, R. J.; Hoekstra, K. K.; Shoup, R. D. U.S. Patent 3,870,658, 1975.
(13) Kummer, J. T. *Adv. Chem. Ser.* **1975**, *No. 143*, 178.
(14) Yu Yao, Y. F. *J. Catal.* **1975**, *39*, 104.
(15) Yu Yao, Y. F.; Kummer, J. T. *J. Catal.* **1977**, *45*, 388.
(16) Severino, F.; Laine, J. *Ind. Eng. Chem. Prod. Res. Dev.* **1983**, *22*, 396.
(17) Severino, F.; Brito, J.; Carias, O.; Laines, J. *J. Catal.* **1986**, *102*, 172.
(18) Laine, J.; Albornoz, A.; Brito, J.; Carias, O.; Castro, G.; Severino, F.; Vaiera, D. In *Catalysis and Automotive Pollution Control*; Crucq, A., Frennet, A., Eds.; Elsevier: Amsterdam, 1987; p 387.
(19) Laine, J.; Severino, F. *Appl. Catal.* **1990**, *65*, 253.
(20) Bijsterbosch, J. W.; Kapteijn, F.; Moulijn, J. A. *J. Mol. Catal.* **1992**, *74*, 193.
(21) Dekker, N. J. J.; Hoorn, J. A. A.; Stegenga, S.; Kapteijn, F.; Moulijn, J. A. *AIChE J.* **1992**, *38*, 385.
(22) Lopez Agudo, A.; Palacios, J. M.; Fierro, J. L. G.; Laine, J.; Severino, F. *Appl. Catal.* **1992**, *91*, 43.
(23) Kapteijn, F.; Stegenga, S.; Dekker, N. J. J.; Bijsterbosch, J. W.; Moulijn, J. A. *Catal. Today* **1993**, *16*, 273.
(24) Stegenga, S.; van Soest, R.; Kapteijn, F.; Moulijn, J. A. *Appl. Catal., B* **1993**, *2*, 257.
(25) Dekker, F. H. M.; Dekker, M. C.; Bliek, A.; Kapteijn, F.; Moulijn, J. *Catal. Today* **1994**, *20*, 409.
(26) Park, P. W.; Ledford, J. S. *Ind. Eng. Chem. Res.* **1998**, *37*, 887.
(27) Hertl, W.; Farrauto, R. J. *J. Catal.* **1973**, *29*, 352.
(28) Yu Yao, Y. F.; Kummer, J. T. *J. Catal.* **1977**, *45*, 388.
(29) Rastogi, R. P.; Singh, G.; Dubey, B. L.; Shukla, C. S. *J. Catal.* **1980**, *65*, 25.
(30) Chien, C. C.; Cheung, W. F.; Hueng, T. J. *Appl. Catal., A* **1995**, *131*, 73.

10.1021/cm001126y CCC: $19.00 © 2000 American Chemical Society
Published on Web 09/20/2000

understood. Many are referred to as "copper chromites", although it is not clear in many cases what is meant by the use of this terminology. Studies of Cu/Cr catalysts have reached a number of empirical conclusions. For instance in such materials copper oxide has been proposed to be the active component for CO oxidation, while chromium oxide has been postulated to perform several functions including limiting catalyst reduction, preventing catalyst poisoning, inhibiting bulk copper aluminate formation, improving thermal stability, and increasing catalyst dispersion.[14,16−18,20,21,24,30,35,38,39] Synergistic effects have been proposed which have been attributed to electronic interactions between the copper and chromium components.[16,20,30] What is also not well understood is the importance of the Cu:Cr ratio for optimum catalytic activity, and ratios of both 2 and 1 have been reported to be the optimum for CO oxidation.[10,17] In a series of Cu/Cr-promoted alumina catalysts, the formation of $CuCr_2O_4$ was demonstrated to give improved CO oxidation activity over CuO, while chromium-rich materials were less active due to the formation of Cr_2O_3.[26]

We have previously reported the nature of both the copper(II)− and chromium−tin(IV) oxide singly promoted catalysts on thermal activation. Prior to thermal activation the Cu(II)/SnO_2 catalyst materials comprise hexaaqua $\{Cu(H_2O)_6\}^{2+}$ cations sorbed onto the surface of small (ca. 1−2 nm) tin(IV) oxide particles. However, calcination at temperatures of ≥873 K causes the phase separation of CuO. At intermediate calcination temperatures, the copper appears to be dispersed as amorphous CuO. Only surface copper(II) is readily reduced on exposure to carbon monoxide, and the principal role of Cu(II) is to facilitate electron transfer; i.e., it abstracts the negative surface charges (formed in the oxygen vacancies following desorption of CO_2) to form Cu(I), which is then oxidized back to Cu(II) by reaction with oxygen.[40,41]Freshly prepared Cr/SnO_2 catalyst materials also comprise small (ca. 1−2 nm) particles of hydrous tin(IV) oxide on the surface of which are sorbed chromate(VI) anions, $\{Cr(H_2O)_6^{3+}\}$ cations, or polymeric γ-CrOOH depending on the preparative route and the source of chromium. In all three cases, however, calcination at 573 K results in the formation of the mixed-valence chromium compound Cr_5O_{12}, although at higher calcination temperatures Cr_2O_3 is formed.[42]

Although it is possible that each promoter in the doubly promoted Cu/Cr/SnO_2 catalyst may behave individually as in the singly promoted catalysts, some interaction is not to be unexpected. To resolve this problem, here we describe the nature of doubly promoted Cu/Cr/SnO_2 catalyst materials prepared by coprecipitation from aqueous solutions containing tin(IV), copper(II), and chromium(III) ions. A priori, it might be expected that coprecipitation from solutions containing more than one metal cation would give rise to an oxide material in which the cations are uniformly dispersed within the freshly precipitated oxide particles. Optimum catalytic activity in catalyst materials such as these is produced via thermal preactivation processing, usually in the temperature range 573−673 K, although heating to much higher temperatures invariably results in significant lowering of activity. Many different changes, both chemical and physical, can occur during such thermal processing including sintering, change in pore texture, migration of heteroions, phase separation, etc. It is, therefore, of critical importance for the understanding of the operation of this type of catalyst system to gain a knowledge of their fundamental constitution and behavior on thermal treatment. Hence in this paper we describe the nature of as-prepared Cu/Cr/SnO_2 catalyst materials as well as after calcination processing using a number of techniques including FT-IR spectroscopy, powder X-ray diffraction, transmission electron microscopy, X-ray photoelectron spectroscopy, and extended X-ray absorption fine structure and near edge structure.

It should be noted, however, that although the catalytic activity of these materials is comparable and, in some circumstances, superior to platinum group metal catalysts, a major concern is the presence of chromium as a promoter. The toxicity, mutagenic effects and carcinogenicity of chromium compounds is well documented, and the adverse health effects suffered by workers exposed to Cr(VI) has also been studied extensively.[43−46] Such factors would most probably have an adverse effect on the commercialization of this particular type of catalyst for automobile purposes. Nevertheless, these data shed important light in the area of transition metal-promoted tin(IV) oxide oxidation catalyst materials.

Experimental Section

Preparation of Catalyst Materials. Catalyst preparation was achieved by a modification of the precipitation method described previously.[42] Both $Cu(NO_3)_3 \cdot 2.5H_2O$ and $Cr(NO_3)_3 \cdot 9H_2O$ in the target atomic ratios were allowed to dissolve and homogenize in the vigorously stirred solution of tin(IV) chloride prior to addition of base. The gelatinous precipitate formed was washed free of chloride ion (silver nitrate solution) by repeated centrifuging and redispersing in triply distilled water. The solid gel obtained was then allowed to air-dry at 333 K for 2−3 days. At this stage the gel was of a granular appearance and approximately one-tenth of its initial volume. These large granules were then broken down by pouring a small amount of triply distilled water over them and then

(31) Heyes, C. J.; Irwin, J. G.; Johnson, H. A.; Moss, R. L. *J. Chem. Technol. Biotechnol.* **1982**, *32*, 1034.
(32) Subbana, P.; Greene, H.; Desal, F. *Environ. Sci. Technol.* **1988**, *22*, 557.
(33) McCabe, R. W.; Mitchell, F. J. *Ind. Eng. Chem. Prod. Res. Dev.* **1983**, *22*, 212.
(34) Rajesh, H.; Ozkan, U. S. *Ind. Eng. Chem. Prod. Res. Dev.* **1993**, *32*, 1622.
(35) Tarasov, A. L.; Osmanov, M. O.; Shveta, V. A.; Kasanskii, V. B. *Kinet. Catal.* **1990**, *31*, 565.
(36) Kapteijn, F.; Stegenga, S.; Dekker, N. J. J.; Bijsterbosch, J. W.; Moulijn, J. A. *Catal. Today* **1993**, *16*, 273.
(37) Stegenga, S.; van Soest, R.; Kapteijn, F.; Moulijn, J. A. *Appl. Catal., B* **1993**, *2*, 257.
(38) Fattakhova, Z. T.; Ukharskii, A. A.; Shiryaev, P. A.; Berman, A. D. *Kinet. Katal.* **1986**, *27*, 884.
(39) Laine, J.; Severino, F. *Appl. Catal.* **1990**, *65*, 253.
(40) Matar, K.; Zhao, D.; Goldfarb, D.; Azelee, W.; Daniell, W.; Harrison, P. G. *J. Phys. Chem. B* **1995**, *99*, 9966.
(41) Zhao, D.; Shane, J. J.; Daniell, W.; Harrison, P. G.; Goldfarb, D. *Appl. Magn. Reson.* **1996**, *10*, 539.
(42) Harrison, P. G.; Lloyd, N. C.; Daniell, W.; Bailey, C.; Azelee, W. *Chem. Mater.* **1999**, *11*, 896.
(43) Langard, S.; Norseth, T. *Handbook on the Toxicology of Metals*; Friberg, L., Nordberg, G. F., Vouk, V., Eds.; Elsevier: Amsterdam, 1986; Chapter 8.
(44) Hayes, R. B. *Sci. Total Environ.* **1988**, *71*, 331.
(45) Sanz, R. *J. Occup. Med.* **1989**, *31*, 1013.
(46) Cieslak-Golonka, M. *Polyhedron* **1995**, *15*, 3667.

Table 1. Analytical and Appearance Data for Cr(III)/Cu(II)/SnO_2 Catalyst Materials

		appearance/calcination temp (K)			
catalyst[a]	obsd stoichiometry[a,b]	333	573	873	1273
Cr(III)/Cu(II)/Sn (60:20:20 Sn:Cr:Cu)	61.1:18.4:20.7 Sn:Cr:Cu (1:0.30:0.34 Sn:Cr:Cu)	dark green	black	black	gray
Cr(III)/Cu(II)/Sn (70:20:10 Sn:Cr:Cu)	70.0:21.0:9.0 Sn:Cr:Cu (1:0.30:0.13 Sn:Cr:Cu)	dark green	black	black	gray
Cr(III)/Cu(II)/Sn (60:10:20 Sn:Cr:Cu)	71.0:9.5:19.5 Sn:Cr:Cu (1:0.13:0.27 Sn:Cr:Cu)	dark green	light green	brown/red	pink/gray

[a] Atom %. [b] Atom:atom ratio in parentheses.

allowed to air-dry further at 333 K for 24 h. The dry gel was then ground into a fine white powder. Materials prepared by this route are referred to as Cr(III)/Cu(II)/SnO_2 with the Sn:Cr:Cu atom ratio denoted in parentheses. Observed and target Sn:Cr:Cu atom ratios for these materials are shown in Table 1.

Catalyst Thermal Pretreatment. Catalyst materials (approximately 2 g aliquots) were calcined in an alumina boat for 24 h using a Vecstar 91e tube furnace at temperatures of 573, 673, 873, 1073, and 1273 K. Many color changes were observed for each sample type (Table 1) indicating various transformations in dopant oxidation state and phase.

Physical and Spectroscopic Measurements. Catalyst stoichiometries were determined by X-ray fluorescence (Philips PW1480 wavelength dispersive instrument).

Infrared spectra were obtained using a Nicolet 20SXC spectrometer. 32 scans were recorded from KBr disk samples at a resolution of 1 cm^{-1}.

Powder X-ray diffraction data was acquired using a Philips X-pert system fitted with a PW 1710 diffractometer control unit with Cu Kα radiation (λ = 1.5405 Å). Representative diffractograms were acquired over 5−80° in 2θ with 0.02° steps and 0.4s acquisition times per step. DICVOL91[47] was used for indexing. Data for Rietveld refinement[48] were acquired between values of 5−120° in 2θ with 0.02° steps and 9.5 s acquisition times per step.

EXAFS measurements were performed on station 8.1 at the Daresbury laboratory, Warrington, U.K., which operates at an energy of up to 2.0 GeV and a maximum beam current of 200 mA. The X-rays are vertically collimated producing a beam of less than 1 mrad divergence. A Si(111) double crystal monochromator was used to select a single-wavelength beam of X-rays; the tuneable energy range that can be achieved using this monochromator is 2−10 keV. A 40−50% amount of the X-ray beam was rejected to filter out the undesired harmonics while retaining 50−60% of the primary beam intensity.

Data were collected at the Cr K-edge (5.989 keV) in fluorescence mode by utilizing a Ge-13 channel solid-state detector. The sample was positioned at ca. 45° to the incident so as to maximize the solid angle seen by the detector. A total of 6 scans were recorded for each catalyst sample, and refinement was achieved using EXBACK, EXCALIB, and EXCURV92.[49] The scans were co-aligned, spikes due to noise removed, and the total number of scans added together to produce a single output data set with an improved signal-to-noise using EXCALIB. Background X-ray absorption was removed from the summed data set in two stages using the program EXBACK. Initially the preedge background was determined by fitting this region to a polynomial usually of order 1. The background absorption was then removed from the postedge region by a series of linked polynomial curves (normally 2 or 3) of order 3. With both the preedge and postedge background absorption removed from the data, the x-axis was converted from energy to k-space ($k = 2\pi/\lambda$, where λ is the electron wavelength) to give the EXAFS oscillations form $k = 0$. The EXAFS were then multiplied to k^3 so as to increase the amplitude of the oscillations at high values of k. Finally, radial distribution spectra were obtained via Fourier transformation of the EXAFS data. EXCURV92 was used to simulate EXAFS spectra of radial shells of neighbors around the central atom. For a more detailed description of the curved wave theory used in the program to calculate theoretical backscattering amplitudes and phase shifts the reader is directed to the publications of Gurman[50] and Lee.[51]

Data were analyzed by taking published structural information from specific possible model compounds, extracting coordination shells and refining just distances and Debye−Waller factors. The significance of extra shells was evaluated using the reduced χ^2 test, $N_p = [\{(2\Delta k \cdot \Delta R)/\pi\} + 1]$, where N_p is the maximum number of variables and Δk and ΔR are the ranges in k- and r-space, respectively.

The estimated levels of accuracy in the refinements made by the EXCURV92 program arising from imperfect transferability of phase shifts and the fitting procedures are the following: coordination number (50%); Debye−Waller factor, $2\sigma^2$ (50%); radii (0.02 Å).

TEM were recorded using a JEOL 2000FX transmission electron microscope at the Department of Materials Engineering and Materials Design, University of Nottingham, operating at an accelerating voltage of 200 kV. Catalyst samples were sonicated in dry chloroform for 15 min, and one drop of the resultant suspension was then allowed to dry upon a holey carbon coated copper TEM grid.

XPS measurements were performed at the Department of Materials Engineering and Materials Design, University of Nottingham, using a VG Ionex spectrometer interfaced with the necessary data handling software. For both material types spectra were recorded under UHV conditions (10^{-8} Torr), using Al Kα primary radiation (13 kV, 20 mA). Data were collected in the sequence of a survey scan (to determine the C 1s reference), followed by scans of the Cr 2p, O 1s, and Sn 3d regions to minimize the time of exposure to X-rays. As the samples were dilute, multiple scans (40) of the Cr 2p region were necessary to facilitate spectra of sufficient intensity to enable sensible deconvolution with the data handling software. Each sample was subjected to an X-ray exposure time of ca. 45 min, which resulted in an approximate photoreduction of 52% of the Cr^{6+} species. After acquisition of spectra, various data handling procedures were carried out on the raw data. To establish peak areas, the spectrum was smoothed and then subjected to a Shirley background subtraction before a normalized peak area could be generated. The peaks during manifold deconvolution were assumed to be Gaussian, and the full width at half-maximum (fwhm) values assigned to them were constrained to be close to the values reported in the literature.[52] This was performed manually before an iterative routine was employed, thus reducing errors by variation of peak attributes (height, width, and position). To compensate for charging effects, which were observed as much as up to +18 eV, binding energies were normalized with respect to the position of the C 1s signal determined from of a survey spectrum and held constant at 285.0 eV.[53]

(47) DICVOL91: Boultif, A.; Louer, D. *J. Appl. Crystallogr.* **1991**, *24*, 987.
(48) PC-Rietveld Plus, Philips, June 1993.
(49) EXBACK, EXCALIB, and EXCURV92: Daresbury Computer programs, Daresbury Laboratory, Cheshire, U.K.
(50) Gurman, S. J.; Binstedt, N.; Ross, I. J. *Phys. C* **1984**, *17*, 143; **1986**, *19*, 1845.
(51) Lee, P. A.; Pendry, J. B. *Phys. Rev. B* **1975**, *11*, 2795.21.
(52) Okamoto, Y.; Fuji, M.; Imanaka, T.; Teranishi, S. *Bull. Chem. Soc. Jpn.* **1976**, *49*, 859.

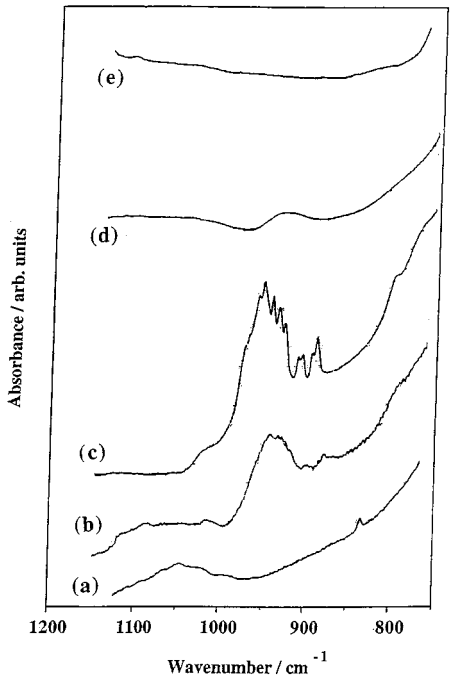

Figure 1. Mid-infrared spectra of the Cr(III)/Cu(II)/SnO_2 (70:20:10 Sn:Cr:Cu) catalyst (a) after drying at 333 K and after calcination at (b) 573 K, (c) 673 K, (d) 873 K, and (e) 1273 K.

Results

Mid-FT-IR Studies. Spectra for the Cr(III)/Cu(II)/SnO_2 (70:20:10 Sn:Cr:Cu) catalyst material exhibit an intense broad envelope of bands for the uncalcined material which can be assigned to the antisymmetric Sn−O−Sn stretching modes of the surface-bridging oxide formed by condensation of adjacent surface hydroxyl groups. The Sn−O−Sn band increases in intensity, sharpens, and shifts to higher wavenumber as the calcination temperature is increased, denoting the strengthening of the Sn−O−Sn bond due to elimination of hydroxyl species.

After calcination at 573−673 K new bands appear at 956, 951, 939, 932, 924, 910, 903, 892, and 885 cm^{-1}, which can be assigned to stretching modes of a chromate(VI) species, but are lost after calcination at temperatures ≥873 K) (Figure 1). Similar behavior has also been observed for Cr(III)/SnO_2 catalysts in which the mixed-valence chromium oxide Cr_5O_{12} is formed after calcination at 573 K. In the present case the fine structure of these bands appears different suggesting different behavior for the Cr(III)/Cu(II)/SnO_2 catalyst materials.

After calcination at 1273 K, several new bands are superimposed upon the Sn−O−Sn envelope. The two bands at 603 cm^{-1} (ν_1) and 521 cm^{-1} (ν_2) are characteristic of tetragonal spinel copper chromite, $CuCr_2O_4$ (cf. lit.[54,55] 602, 521 cm^{-1}). The same bands at 603 and 522 cm^{-1} characteristic of the $CuCr_2O_4$ phase are also observed in the infrared spectrum of the Cr(III)/Cu(II)/SnO_2 (60:20:20 Sn:Cr:Cu) catalyst material after calcination at 1273 K (Figure 2a). However, different behavior is apparent for the Cr(III)/Cu(II)/SnO_2 (70:10:20 Sn:Cr:Cu) catalyst material calcined at 1273 K (Figure 2b); the characteristic spinel bands are absent, and new band maxima are observed centered at 612, 568, and 539 cm^{-1}.

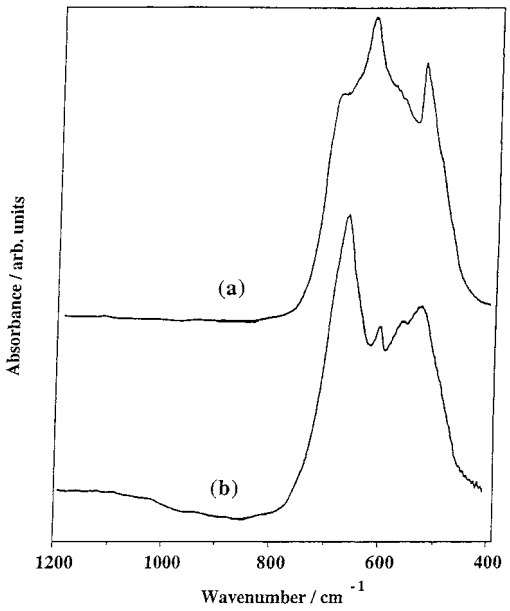

Figure 2. Mid-infrared spectra of the Cr(III)/Cu(II)/SnO_2 60:20:20 Sn:Cr:Cu (a) and 70:20:10 Sn:Cr:Cu (b) catalysts after calcination at 1273 K.

X-ray Diffraction Studies. Prior to calcination, all of the Cr(III)/Cu(II)/SnO_2 materials exhibit diffractograms comprising four very broad peaks due to small particulate SnO_2. As previously seen for the singly promoted Cr(III)/SnO_2[42] catalyst materials, these peaks progressively increase in intensity and sharpen with increasing calcination temperature, indicating an increase in crystallinity.

XRD diffractograms for the Cr(III)/Cu(II)/SnO_2 (60:20:20 Sn:Cr:Cu) catalyst material after calcination at temperatures in the range 873−1273 K exhibit peaks due to tetragonal SnO_2 (major phase) and also to the spinel $CuCr_2O_4$[56] (Figure 3A) This latter phase is observed initially after calcination at 873 K and was identified uneqivocally by Rietveld analysis of the material calcined at 1273 K. Diffractograms for the chromium-rich Cr(III)/Cu(II)/SnO_2 (70:20:10 Sn:Cr:Cu) catalyst also show the presence of $CuCr_2O_4$ after calcination at temperatures ≥873 K along with phase-separated Cr_2O_3 (Figure 3B). Similar observations have been made by Castiglioni et al.[57] for various copper−zinc−cadmium chromite catalysts. Converse behavior is observed after calcination of the copper-rich Cr(III)/Cu(II)/SnO_2 (70:10:20 Sn:Cr:Cu) catalyst where phase-separated $CuCr_2O_4$ is again observed after calcination at temperatures of 873−1073 K accompanied by small amounts of phase-separated CuO (Figure 3C). However, after calcination at 1273 K, a new phase is formed identified as copper chromate, $Cu_2Cr_2O_4$, which possesses a spinel-like structure with the most intense peaks at interplanar spacings (d/Å) of {006} (2.851), {101} (2.549), {012} (2.468), {104} (2.207), {018} (1.645),

(53) Best, S. A.; Squires, R. G.; Walton, R. A. *J. Catal.* **1977**, *47*, 292.
(54) Hafner, S. *Z. Kristallogr.* **1961**, *115*, 331.
(55) Basak, D.; Ghose, J. *Spectrochim. Acta, Sect. A* **1994**, *50*, 713.
(56) JCPDS Pattern No. 34-424 ($CuCr_2O_4$).
(57) Castiglioni, G. L.; Vaccari, A.; Fierro, G.; Inversi, M. *Appl. Catal., A* **1995**, *123*, 123.

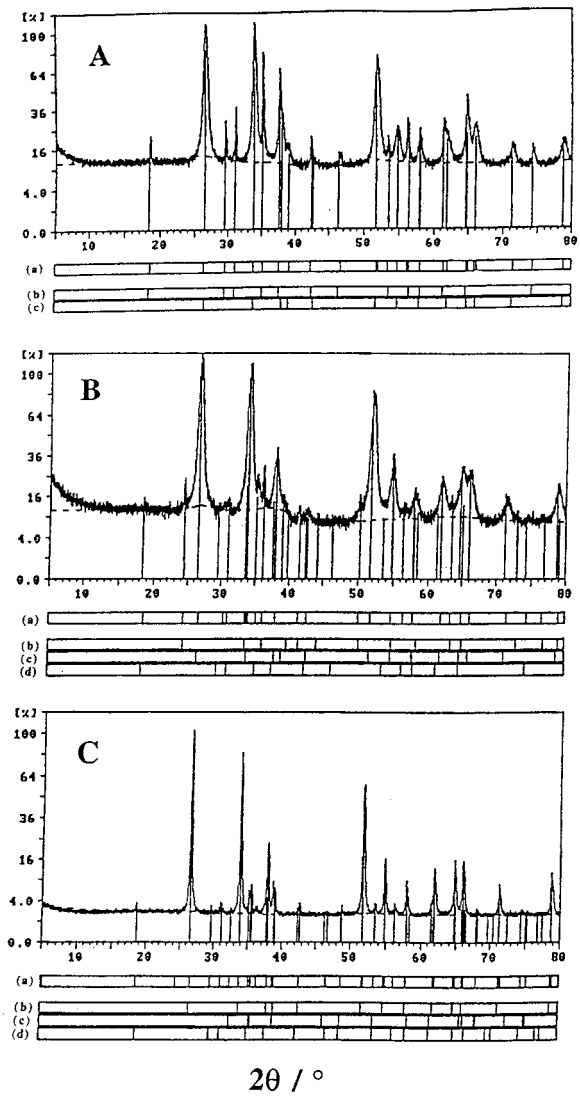

Figure 3. Powder X-ray diffractograms of Cr(III)/Cu(II)/SnO_2 (60:20:20 Sn:Cr:Cu) after calcination at 873 K (A) (tickmarks show peaks positions for (a) catalyst, (b) $CuCr_2O_4$, and (c) SnO_2), Cr(III)/Cu(II)/SnO_2 (70:20:10 Sn:Cr:Cu) after calcination at 873 K (B) (tickmarks show peaks positions for (a) catalyst, (b) Cr_2O_3, (c) SnO_2, and (d) $CuCr_2O_4$), and Cr(III)/Cu(II)/SnO_2 (70:10:20 Sn:Cr:Cu) (C) (tickmarks show peaks positions for (a) catalyst, (b) SnO_2, (c) CuO, and (d) $CuCr_2O_4$), catalysts after calcination at 1073 K.

and {110} (1.488),[58] although phase-separated monoclinic CuO can still be detected in the material after this calcination treatment.

Investigations into the possibility of solid solution behavior were made by indexing (DICVOL91[47]) and refining the XRD patterns by the Rietveld[48] method. The indexed values and refinement parameters for both materials are in good agreement ($a \pm 0.004$ Å and $c \pm 0.005$ Å) with the literature.[59−61] Therefore, it can be concluded that the chromium and copper promoter species exist solely as phase-separated $CuCr_2O_4$, $Cu_2Cr_2O_4$, Cr_2O_3, and CuO at elevated calcination temperatures with no incorporation of either heteroatom into the tin(IV) oxide lattice induced by thermal treatment.

(58) JCPDS Pattern No. 39-247 ($Cu_2Cr_2O_4$).
(59) JCPDS Pattern No. 21-1250 (SnO_2).
(60) JCPDS Pattern No. 38-1479 (Cr_2O_3).
(61) Baur, W. H.; Khan, A. A. *Acta Crystallogr., B* **1971**, *27*, 2133.

Table 2 details the values of mean crystallite sizes determined using the Scherrer equation for the SnO_2 particles for all three Cr(III)/Cu(II)/SnO_2 stoichiometries over a range of calcination temperatures. Little increase in crystallite size is observed for all materials up to calcination temperatures of 873 K, but large increases in crystallite size occur thereafter. All three materials increase in particle size by ca. 100× after calcination at 1273 K, with the exception of the material containing excess copper where an increase of ca. 220× is seen. This behavior is similar to that observed for both singly promoted Cr(III)/SnO_2[42] and Cu(II)/SnO_2[62] catalyst materials, and all three types of catalysts exhibit comparable mean SnO_2 particle sizes in the range of 1−3 nm for calcination temperatures below 873 K.

Transmission Electron Microscopy. TEM examination of the Cr(III)/Cu(II)/SnO_2 (60:20:20 Sn:Cr:Cu) catalyst material showed it to be generally amorphous in nature in the calcination temperature range 333−673 K (Figure 4a), with particle sizes ranging from 1.5 nm (333 K) up to 2.5 nm (673 K) in dimension. Little change is observed after calcination at 573 K (Figure 4b), but some agglomeration is seen after calcination at 673 K (Figure 4c) and the catalyst material now comprises a range of particle sizes. A large increase in particle size is observed after calcination at temperatures ≥873 K, with a wide variation in size (mean ca. 20 nm) (Figure 4d). After calcination at 1073 K the particles have the appearance of rounded hexagons and are much larger (Figure 4e), while calcination at 1273 K produces globular particles which are ca. 120 times greater in size than the uncalcined material (Figure 4f). Lattice fringing can be seen in the samples calcined at high temperature, indicating a high degree of crystallinity as shown in the XRD diffractograms. Throughout EDXA analysis corroborates the uniformity of the Sn, Cr, and Cu compositions, in good agreement with the XRF elemental analysis.

Overall, there is a good agreement with the observed particle sizes determined by TEM with those calculated from X-ray line broadening (Table 2). The materials appear homogeneous at each calcination temperature, and no phase separation may be readily distinguished (cf. the XRD data at higher calcination temperatures).

EXAFS Studies. EXAFS spectra for Cr(III)/Cu(II)/SnO_2 (70:10:20 Sn:Cr:Cu) catalyst material for various calcination treatments are shown in Figure 5. As was previously[42] observed for the Cr/SnO_2 catalysts, a pre-edge peak is observed in the XANES region at ca. +4.1−4.3 eV from the Cr K-edge after calcination at 573 K, although it is absent at lower and also at higher calcination temperatures. The nature of this peak has been discussed previously[42] and is due to the presence of tetrahedrally coordinated Cr^{6+} species, and arises from a dipole-allowed 1s → 3d electronic transition. Hence, it is inferred that oxidation of the chromium(III) component to chromium(VI) occurs under these relatively mild conditions.

After calcination at 573 K, the EXAFS data (Table 3) indicate a tetrahedral four-coordination for chromium typical of the Cr^{6+} valence state consistent with the observation of the pre-edge feature. XPS data show that

(62) Harrison, P. G.; Bailey, C.; Ball. I.; Daniell, W.; Zhao, D.; Goldfarb, D.; Lloyd, N. C.; Azelee, W. *Chem. Mater.* **1999**, *11*, 3643.

Table 2. Mean Crystallite Sizes for Cr(III)/Cu(II)/SnO_2 Catalyst Materials after Calcination at Temperatures in the Range 333−1273 K

	mean particle size (D)/nm					
material	333 K	573 K	673 K	873 K	1073 K	1273 K
60:20:20 Sn:Cr:Cu[a]	1.3	1.3	1.7	16.5	36.4	149.4
60:20:20 Sn:Cr:Cu[b]	1.5 ± 0.5	1.5 ± 0.5	2.0 ± 5	25 ± 8	40 ± 20	180 ± 20
70:20:10 Sn:Cr:Cu[a]	1.2	1.3	2.1	13.1	34.2	118.6
70:10:20 Sn:Cr:Cu[a]	1.3	1.3	2.5	15.9	88.2	289.6

[a] From X-ray line broadening. [b] From TEM micrographs. Errors are averaged from 5 micrographs.

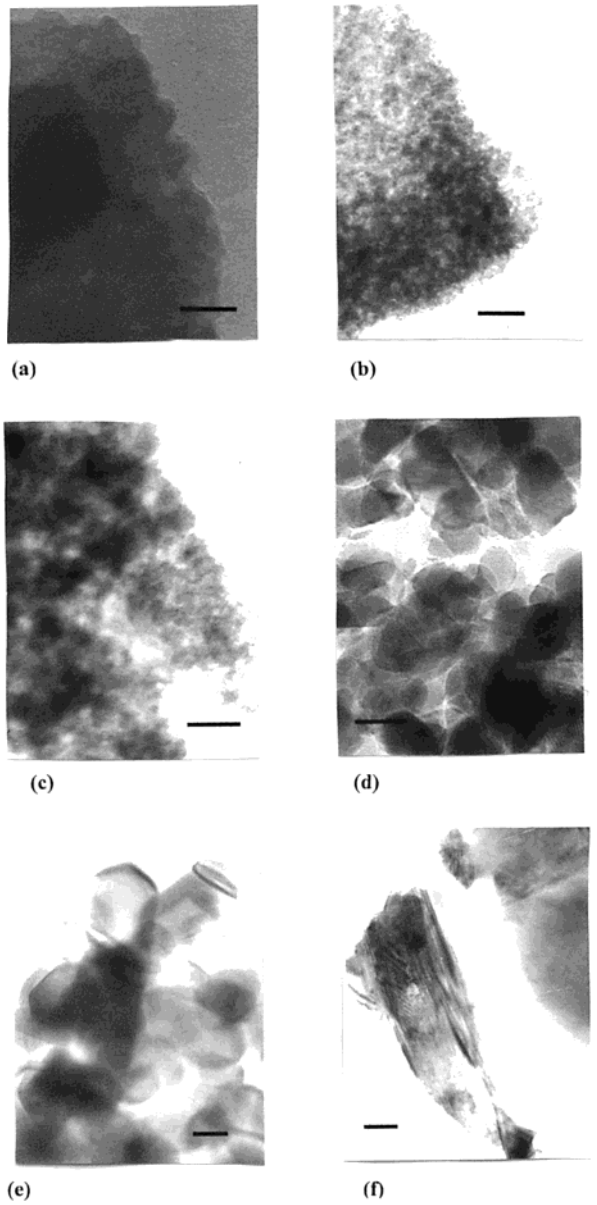

Figure 4. Transmission electron micrographs of Cr(III)/Cu(II)/SnO_2 (60:20:20 Sn:Cr:Cu) after calcination at (a) 333 K, (b) 573 K, (c) 673 K, (d) 873 K, (e) 1073 K, and (f) 1273 K. All scale bars represent 20 nm.

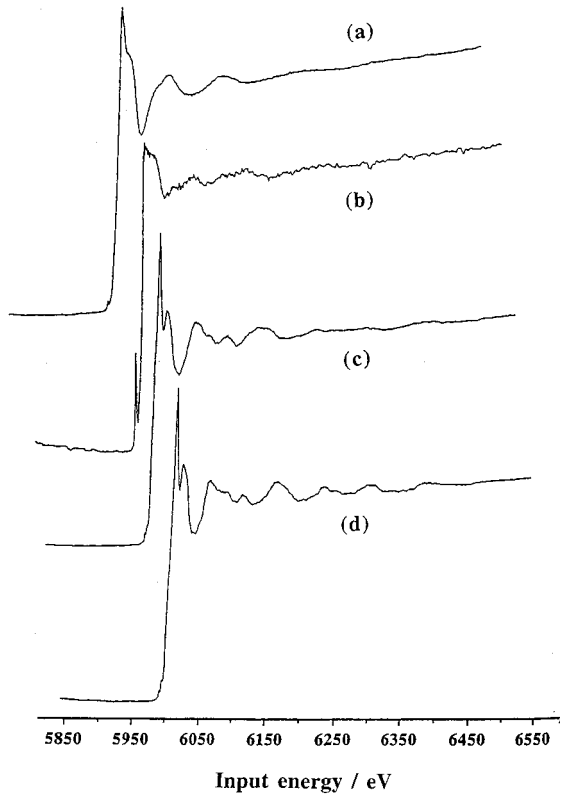

Figure 5. Cr K-edge EXAFS spectra for Cr(III)/Cu(II)/SnO_2 (70:10:20 Sn:Cr:Cu) after (a) drying at 333 K and after calcination at (b) 573 K, (c) 1073 K, and (d) 1273 K. Spectra are not energy calibrated, and spectra (a)−(c) are offset to lower energy with respect to spectrum d by ca. 100 eV.

only chromium(VI) is present after thermal processing at these temperatures (see later). Surface-adsorbed chromate(VI) species on tin(IV) oxide do not survive thermal processing at these temperatures but are transformed into the mixed-valence compound Cr_5O_{12}. The same species is also formed by thermal treatment of Cr(III)/SnO_2 materials.[42] However, in the present case, the absence of oxygen shells at ca. 2 Å precludes Cr_5O_{12}. The most likely candidate is copper(II) chromate(VI), $CuCrO_4$, which comprises distorted $\{CrO_4\}$ tetrahedra with Cr−O bond lengths of 1.602 and 1.731 Å connected by slightly irregular bridging $\{CuO_6\}$ octahedra. The same phase is also present in the 60:20:20 Sn:Cr:Cu material calcined at 573 K, and in both cases the high R values ($R = 61$) can be attributed to the noise in the EXAFS oscillations, $\chi(k)$. Nevertheless, the radial distances for both specimens analyzed after calcination at 573 K are in good agreement with the literature.

Powder XRD studies show that, at calcination temperatures of ≥873 K, the promoting chromium and copper species exist as phase-separated $CuCr_2O_4$ for all three stoichiometries. For the Cr(III)/Cu(II)/SnO_2 (70:10:20 Sn:Cr:Cu) material, this phase is identifiable in the EXAFS after calcination at 1073 K (Table 3). However, with the copper-rich (70:10:20 Sn:Cr:Cu) catalyst material, calcination at temperatures >1173 K results in the transformation of copper chromite, $CuCr_2O_4$, into crystalline $Cu_2Cr_2O_4$. Powder XRD studies show that small amounts of phase-separated CuO also exist after calcination at 1273 K.

Table 3. Refined[a] Structural Parameters from Cr K-Edge EXAFS Data for the Cr(III)/Cu(II)/SnO_2 (70:10:20 Sn:Cr:Cu) Catalyst after Calcination at Temperatures in the Range 573−1273 K

calcination temp (K)	atom type	coord no.	Debye−Waller factor $2\sigma^2$/Å^2	radial dist/Å	Cr species present	lit. values/Å
573	O	2	0.022	1.602	$CuCrO_4$[b]	1.599
	O	2	0.013	1.752		1.731
	Cu	4	0.011	3.328		3.301
	O	4	0.010	3.411		3.406
1073	O	6	0.005	1.977	$CuCr_2O_4$[c]	2.000
	Cr	4	0.005	2.911		2.896
	Cr	2	0.007	3.041		3.035
	Cu	2	0.021	3.128		3.289
	O	2	0.009	3.298		3.310
1273	O	6	0.007	1.982	$Cu_2Cr_2O_4$[d]	1.989
	Cr	6	0.007	2.986		2.975
	Cu	6	0.019	3.313		3.327
	O	6	0.045	3.620		3.580
	Cu	6	0.020	4.452		4.463

[a] R values 61.0 (573 K), 30.0 (1073 K), and 32.0 (1273 K). [b] References 63 and 64. [c] References 64 and 65. [d] References 64 and 66.

Table 4. Parameters Obtained by Deconvolution of the Cr 2p Doublet in the XPS Spectra of the Cr(III)/Cu(II)/SnO_2 Catalyst after Calcination at Temperatures in the Range 333−1273 K

catal mater	pretreatment temp/K	binding energy/eV[a] $2p_{3/2}$	binding energy/eV[a] $2p_{1/2}$	ΔE_{so}/eV	$2p_{3/2}$ area /counts	assgnt
Cr(III)/Cu(II)/SnO_2 (60:20:20 Sn:Cr:Cu)	333	577.0 (3.5)	586.8 (3.5)	9.8	2370	Cr^{3+}
		579.4 (3.8)	590.2 (3.8)	10.8		Cr^{3+} sat.
	673	577.4 (3.4)	586.4 (3.4)	9.0	2377	Cr^{5+}
		580.5 (3.8)	589.6 (3.9)	9.1		Cr^{6+}
	873	576.7 (3.7)	586.4 (3.6)	9.7	2664	Cr^{3+}
		579.8 (3.8)	590.5 (3.9)	0.7		Cr^{3+} sat.
	1273	576.5 (3.6)	586.4 (3.6)	9.8	2840	Cr^{3+}
		579.0 (3.8)	589.8 (3.9)	10.8		Cr^{3+} sat.
Cr(III)/Cu(II)/SnO_2 (70:10:20 Sn:Cr:Cu)	333	577.0 (3.2)	586.8 (3.5)	9.8	1265	Cr^{3+}
		579.4 (3.6)	590.1 (3.5)	10.7		Cr^{3+} sat.
	573	577.7 (3.5)	586.7 (3.5)	9.0	1431	Cr^{5+}
		580.4 (3.9)	589.7 (3.8)	9.3		Cr^{6+}
	673	577.5 (3.5)	586.6 (3.4)	9.1	1502	Cr^{5+}
		580.4 (3.7)	589.4 (3.9)	9.0		Cr^{6+}
	873	576.6 (3.5)	586.3 (3.4)	9.7	1543	Cr^{3+}
		579.7 (3.8)	590.6 (3.9)	10.7		Cr^{3+} sat.
	1073	576.6 (3.4)	586.4 (3.6)	9.8	1676	Cr^{3+}
		579.9 (4.0)	590.6 (3.9)	10.7		Cr^{3+} sat.
	1273	576.4 (3.4)	586.2 (3.5)	9.8	1715	Cr^{3+}
		579.5 (4.1)	590.3 (3.9)	10.8		Cr^{3+} sat.

[a] FWHM in parentheses.

Calcination at 1273 K results in the formation of the crystalline $CuCr_2O_4$ phase for both the 60:20:20 Sn:Cr:Cu and 70:20:10 Sn:Cr:Cu Cr(III)/Cu(II)/SnO_2 catalyst materials again corroborating the XRD analyses. XRD has shown that for the chromium-rich Cr(III)/Cu(II)/SnO_2 (70:20:10 Sn:Cr:Cu) catalyst a small amount of phase-separated Cr_2O_3 is present after calcination at 1273 K. Consequently, slightly shorter radial distances than expected result for the $CuCr_2O_4$ phase due to a contribution from small amounts of phase-separated Cr_2O_3.

XPS Studies. The background and interpretation of Cr 2p spectra have been described in detail previously.[67] Chromium in either the 3+ and 6+ oxidation states may be distinguished in terms of binding energy, the satellite structure, the spin−orbit intensity ratio, and the spin−orbit splitting. However, caution needs to be exercised in the qualitative analysis of the Cr 2p level for Cr^{6+} compounds due to photoreduction of Cr^{6+} to Cr^{5+} by the X-ray flux during data collection. The result is a decrease in intensity of the peak due to Cr 2p of Cr^{6+} with exposure time while concurrently a new Cr 2p peak, having a lower binding energy value, appears with increasing intensity. Thus, information about the binding energy and the spin−orbit splitting are used in order to distinguish the valence states of chromium-promoted tin(IV) oxide catalyst materials.

Binding energy and spin−orbit splitting data of the Cr 2p region for both Cr(III)/Cu(II)/SnO_2 (60:20:20 Sn:Cr:Cu and 70:10:20 Sn:Cr:Cu) catalyst materials are collected in Table 4, and smoothed, deconvoluted Cr 2p regions after various thermal treatments for the Cr(III)/Cu(II)/SnO_2 (60:20:20 Sn:Cr:Cu) catalyst are shown in Figure 6a−d.

For both catalyst materials dried at 333 K, the Cr 2p doublet can be resolved into four individual peaks (Figure 6a). The maximal peaks (Cr $2p_{3/2}$, 577.0 eV) in

(63) Åsbrink, S.; Norrby, L. J. *Acta Crystallogr., Sect. B*. **1970**, *26*, 8.
(64) Blake, A. J. Private communication.
(65) Prince, E. *Acta Crystallogr*. **1957**, *10*, 554.
(66) Hannhauser, W.; Vaughn, P. A. *J. Am. Chem. Soc.* **1955**, *77*, 896.
(67) Harrison, P. G.; Daniell, W.; Lloyd, N. C. *J. Phys. Chem. B* **1998**, *102*, 10672.

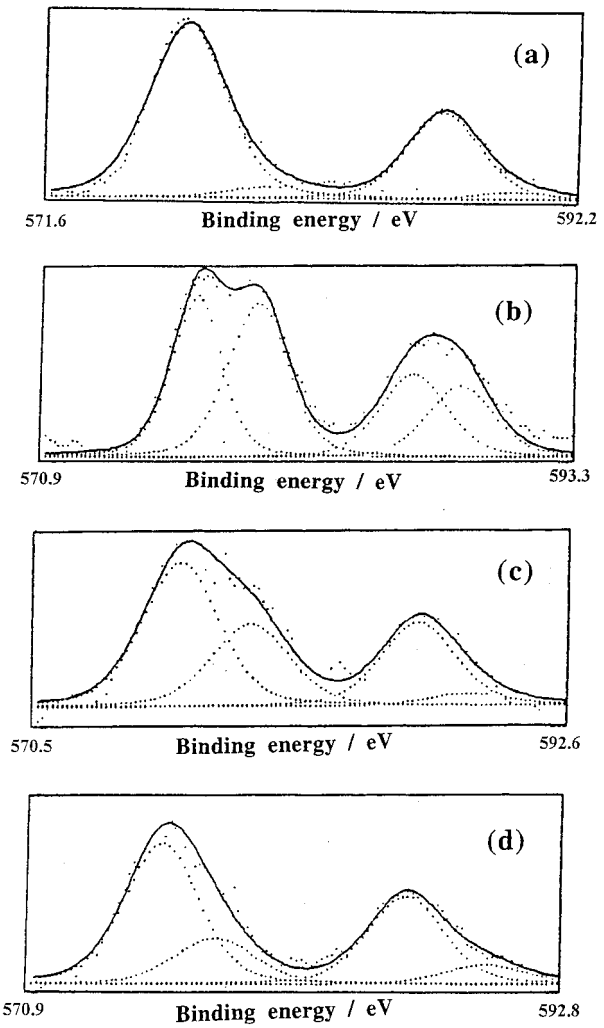

Figure 6. Smoothed and deconvoluted XPS spectra of the Cr 2p doublet for$Cr(III)/Cu(II)/SnO_2$ (60:20:20 Sn:Cr:Cu) after (a) drying at 333 K and after calcination at (b) 673 K, (c) 873 K, and (d) 1273 K.

both manifolds exhibit a spin−orbit splitting of 9.8 eV characteristic of a Cr^{3+} species with the binding energy position in good agreement with studies by Brooks et al. (577.0 eV).[68] Analysis of the O 1s peak (see later) further supports this assignment. The peaks at a slightly higher binding energy to the maximal peaks have a spin−orbit splitting of 10.7/8 eV which corresponds to the Cr^{3+} satellite.

After calcination at 573 and 673 K, four peaks can again be resolved within the Cr 2p doublet, both with (E_{so} values of ca. 9.0 eV, much lower than that expected for Cr^{3+} (ca. 9.8 eV) (Figure 6b). The peak at higher binding energy in each manifold (ca. 580 eV Cr $2p_{3/2}$, 589 eV Cr $2p_{1/2}$) is assigned to the Cr^{6+} present in the previously characterized $CuCrO_4$ phase which remains unaffected by photoreduction in the X-ray flux. The peaks at lower binding energy in each manifold (ca. 577 eV Cr $2p_{3/2}$, 586 eV Cr $2p_{1/2}$) are assigned to the resultant Cr^{5+} species formed by photoreduction of the Cr^{6+} species in $CuCrO_4$ under UHV conditions. The binding energy positions and spin−orbit splittings for both valence states are in good agreement with literature values.[68]

After calcination at 873 K the binding energy positions and spin−orbit splittings for the peaks in the Cr 2p manifolds are all in accordance with Cr^{3+} being the sole chromium valence state present in the $Cr(III)/Cu(II)/SnO_2$ catalyst materials. The assignments cannot, however, be assigned unequivocally to a specific phase. Nevertheless, the spin−orbit splittings of 9.8 eV for the maximal peak and 10.7/8 eV for the satellite are indicative of Cr^{3+}. EXAFS analysis on these materials has shown that copper chromite ($CuCr_2O_4$), where chromium exists in a +3 valence state, readily forms after calcination at this temperature via a transformation from crystalline $CuCrO_4$.

In the case of the $Cr(III)/Cu(II)/SnO_2$ (60:20:20 Sn:Cr:Cu) material, the $CuCr_2O_4$ phase is still believed to be present in the material after calcination at 1273 K as evidenced by EXAFS and XRD data. However, these two techniques have both demonstrated that when copper is present in excess of chromium (i.e. the 70:10:20 Sn:Cr:Cu material), calcination at 1273 K results in the formation of the $Cu_2Cr_2O_4$ phase. The binding energy position in the Cr $2p_{3/2}$ manifold (576.4 eV) for this system after calcination at 1273 K is in good agreement with that of Allen and Tucker (576.4 eV)[69] for $Cu_2Cr_2O_4$. However, as the difference between this binding energy and that obtained for this system after calcination at 1073 K (576.6 eV, due to $CuCr_2O_4$, characterized by EXAFS and XRD) is negligible (ca. 0.1−0.2 eV), the XPS does not provide conclusive evidence for the existence of the $Cu_2Cr_2O_4$ phase. This is because of the high charging effects observed with all tin(IV) oxide based materials. Nevertheless, the EXAFS and XRD provide conclusive evidence that this phase does indeed exist after calcination at elevated temperatures.

Peak areas under the Cr $2p_{3/2}$ manifold increase progressively as the calcination range up to 1273 K is ascended. Since peak intensities in XPS are directly related to surface (1−10 nm depth) concentration, this may be interpreted as a reflection of dopant migration to the surface and aggregation as the crystallite sizes of the copper/chromium phase-separated species increase with increased calcination temperature. This effect is accompanied by a decrease in the Sn $3d_{5/2}$ peak area for the Sn 3d doublet region above 873 K as illustrated in Table 5 as surface coverage of SnO_2 particles by the secondary phase(s) increases. The binding energy positions are in good agreement with those of Ansell et al. ($3d_{5/2}$, 486.3 eV).[70]

Data from the O 1s region (Table 6) support the observations made in the Cr 2p doublet region. Two peaks can be fitted in the O 1s peak for both uncalcined $Cr(III)/Cu(II)/SnO_2$ materials (Figure 7a), with the maximal peak at ca. 530 eV corresponding to tin(IV) oxide lattice oxygen. The second peak at higher binding energy (ca. 532 eV) is characteristic of surface hydroxyl oxygen species, present on tin(IV) oxide. At calcination temperatures of ≥573 K (Figure 7b), three peaks can be fitted into the O 1s peak for both materials, with the two higher energy peaks assigned as before. The peak

(68) Brooks, A. R.; Clayton, C. R.; Doss, K.; Lu, Y. C. *J. Electrochem. Soc.* **1986**, *133*, 2459.
(69) Allen, G. C.; Tucker, P. M. *Inorg. Chim. Acta* **1976**, *10*, 41.
(70) Katayama, A. *J. Phys. Chem.* **1980**, *84*, 376.

Table 5. Parameters Obtained by Deconvolution of the Sn 3d Doublet in the XPS Spectra for the Cr(III)/Cu(II)/SnO_2 Catalyst after Calcination at Temperatures in the Range 333−1273 K

catal mater	pretreatment temp/K	binding energy/eV[a]		Sn $3d_{5/2}$ area /counts
		$3d_{5/2}$	$3d_{3/2}$	
Cr(III)/Cu(II)/SnO_2	333	486.1 (2.3)	494.6 (2.1)	1464
(60:20:20 Sn:Cr:Cu)	673	486.2 (2.2)	494.5 (2.0)	2875
	873	486.0 (2.3)	494.3 (2.2)	4091
	1273	486.2 (2.3)	494.4 (2.2)	3648
Cr(III)/Cu(II)/SnO_2	333	486.3 (2.2)	494.8 (2.1)	2013
(70:10:20 Sn:Cr:Cu)	573	486.1 (2.2)	494.4 (2.1)	2288
	673	486.4 (2.2)	494.7 (2.1)	3990
	873	486.4 (2.3)	494.6 (2.2)	4265
	1073	486.3 (2.2)	494.6 (2.1)	3020
	1273	486.4 (2.1)	494.6 (1.9)	2874

[a] FWHM in parentheses.

Table 6. Parameters Obtained by Deconvolution of the O 1s Peak in the XPS Spectra for the Cr(III)/Cu(II)/SnO_2 Catalyst after Calcination at Temperatures in the Range 333−1273 K

catal mater	pretreatment temp/K	O 1s binding energy/eV[a]		
Cr(III)/Cu(II)/SnO_2	333		530.3 (2.4)	531.7 (2.2)
(60:20:20 Sn:Cr:Cu)	673	528.9 (2.0)	530.4 (2.2)	531.9 (2.0)
	873	529.2 (2.0)	530.2 (2.0)	531.8 (2.0)
	1273	529.3 (1.9)	530.4 (2.0)	532.0 (2.4)
Cr(III)/Cu(II)/SnO_2	333		530.4 (2.2)	531.9 (2.2)
(70:10:20 Sn:Cr:Cu)	573	528.8 (2.0)	530.4 (2.2)	531.8 (2.0)
	673	528.9 (1.9)	530.3 (2.0)	531.9 (2.1)
	873	528.1 (2.0)	530.4 (2.0)	532.0 (2.1)
	1073	529.2 (1.8)	530.2 (1.9)	531.8 (2.2)
	1273	529.3 (2.0)	530.4 (2.0)	532.0 (2.0)

[a] FWHM in parentheses.

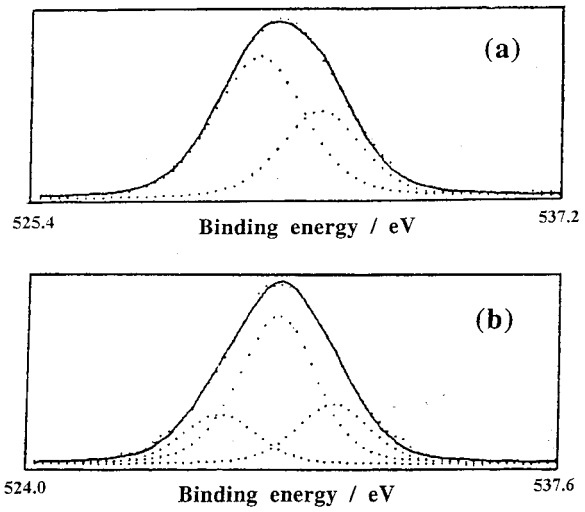

Figure 7. Smoothed and deconvoluted O 1s XPS spectra of for Cr(III)/Cu(II)/SnO_2 (70:10:20 Sn:Cr:Cu) after (a) drying at 333 K and (b) after calcination at 573 K.

at lower binding energy to the tin(IV) oxide lattice oxygen peak becomes marginally greater in energy (528.8 → 529.3 eV) as previously observed for the chromium-promoted tin(IV) oxide catalysts. This is in accordance with oxygen ions in a phase containing Cr^{6+} (in this instance $CuCrO_4$) thermally transforming to a phase containing Cr^{3+} ($CuCr_2O_4$/$Cu_2Cr_2O_4$).

Discussion

Doubly promoted Cu/Cr/SnO_2 catalysts with approximate Cu:Cr atomic ratios of 2, 1, and 0.5 were prepared by coprecipitation from aqueous solutions containing Sn^{4+}, Cu^{2+}, and Cr^{3+} ions in the appropriate ratio. After being dried at 333 K, all three gels were dark green in appearance, and the analytical data shown in Table 1 confirm that the metal ratios determined for the gels were acceptably close to the "target" ratios. Upon calcination, however, the copper-rich gel behaves differently from the other two, becoming pale green at 573 K, brown/red at 873 K, and pink/grey at 1273 K. The other two materials become black at 573 K before turning grey at 1273 K. Up to calcination temperatures of ≈673 K the materials appear homogeneous, comprising small (ca. 1−2 nm) particles of tin(IV) oxide, but by 873 K an increase in size of ca. 1 order of magnitude occurs.

Optimum catalytic performance of Cu/Cr-promoted tin(IV) oxide materials for CO and propane oxidation is achieved after thermal activation in air in the temperature range 573−673 K.[8,71] The data presented here show that at this temperature the two promoting elements interact forming copper(II) chromate(VI), $CuCrO_4$. That the $CuCrO_4$ phase cannot be detected in the powder X-ray diffractograms indicates that it is amorphous in nature. Further, the uniformity of the unit cell data for the SnO_2 crystallites at calcination temperatures ≥873 K show that no significant penetration of copper or chromium into the rutile crystal lattice of the tin(IV) oxide occurs. We, therefore, propose that it is this composite oxide material comprising microparticulate $CuCrO_4$ dispersed on particulate tin(IV) oxide which is the active catalyst.

Although these materials still exhibit very good activity toward the catalytic oxidation of CO and propane after calcination at temperatures ≥873 K,[71] it

(71) Harrison, P. G.; Azelee, W.; Mubarak, A. T.; Bailey, C.; Daniell, W.; Lloyd, N. C. *Catalysis and Automotive Pollution Control IV*, *Studies in Surface Science and Catalysis*; Delmon, B., Yates, J. T., Eds.; Elsevier: Amsterdam, 1998; Vol. 116, p 495.

is nevertheless significantly lower than the activity shown by materials after thermal activation at 673 K. For example, the 60:20:20 Sn:Cu:Cr catalyst achieves total conversion of a 5% CO/air mixture at ambient temperature for the 673 K calcined catalyst, whereas calcination at 873 and 1273 K raises the temperature for complete conversion to 348 and 448 K, respectively. The corresponding temperatures for the total oxidation of a 0.8% propane/air mixture over the same catalyst are 518, 538, and 618 K, respectively.

Both physical and chemical changes occur on heating these materials at temperatures ≥873 K. At these temperatures a progressive increase in particle size occurs which accelerates rapidly with temperature accompanied by a decrease in surface area. This in itself would be expected to lead to a lowering of catalytic activity, but in addition the chemical nature of the materials changes. At these high temperatures only crystalline tin(IV) oxide and copper(II) chromite(III), $CuCr_2O_4$, are observed in the 60:20:20 Sn:Cu:Cr catalyst material. Thus, we conclude that the copper which is not observed must be present as an amorphous oxide-like state. Similarly, for the catalyst materials which are either copper-rich (70:20:10 Sn:Cu:Cr) or chromium-rich (70:10:20 Sn:Cu:Cr), $CuCrO_4$ appears to be the only phase present after calcination at 573 K and the excess copper or chromium, respectively, must also be present as an amorphous oxide-like state. Copper(II) chromite-(III), $CuCr_2O_4$, is also formed in both the copper-rich and the chromium-rich materials after calcination at temperatures in excess of 873 K, and phase-separated crystalline CuO and Cr_2O_3, respectively, are formed. The copper(II) chromite(III), $CuCr_2O_4$, formed in the stoichiometric and chromium-rich materials is unchanged during calcination at temperatures up to 1273 K. However, at this temperature the copper-rich material undergoes a tranformation to copper(I) chromite(III), $Cu_2Cr_2O_4$.

Broadly similar behavior is exhibited by copper and chromium supported on alumina. Studies by Chien et al.[30] have shown that crystalline $CuCrO_4$ exists in Cu/Cr/γ-alumina catalysts after thermal treatment at 573 K. Decomposition of neat $CuCrO_4$ into amorphous $CuCr_2O_4$ is known to occur at a somewhat higher temperature range of 753−773 K.[72] Copper chromite, $CuCr_2O_4$, is also formed on γ−alumina impregnated with copper(II) and chromium(III) solutions and calcined at 773 K, together with CuO and Cr_2O_3 depending on the relative levels of the two promoters.[26] With an excess of copper in Cu/Cr/γ-alumina catalysts phase transformations from the $CuCr_2O_4$ spinel to $Cu_2Cr_2O_4$ occur readily after calcination at 1173 K.[30,73−75]

Conclusions

Doubly promoted Cu/Cr/SnO_2 catalysts with approximate Cu:Cr atomic ratios of 2, 1, and 0.5 may be prepared by coprecipitation from aqueous solutions containing Sn^{4+}, Cu^{2+}, and Cr^{3+} ions in the appropriate ratio. The materials produced are homogeneous up to calcination temperatures of ≈673 K, comprising small (ca. 1−2 nm) particles of tin(IV) oxide, but by 873 K an increase in size of ca. 1 order of magnitude occurs.

After thermal activation in air in the temperature range 573−673 K the two promoting elements interact forming copper(II) chromate(VI), $CuCrO_4$, with no significant penetration of copper or chromium into the rutile crystal lattice of the tin(IV) oxide. This composite oxide material comprising microparticulate $CuCrO_4$ dispersed on particulate tin(IV) oxide appears to be the active catalyst for CO and propane oxidation.

At temperatures ≥873 K a progressive increase in particle size occurs which accelerates rapidly with temperature, and the spinel phase $CuCr_2O_4$ is formed in all three systems, together with Cr_2O_3 when excess chromium is present and CuO when excess copper is present. At 1273 K, however, the copper-rich material undergoes a tranformation to copper(I) chromite(III), $Cu_2Cr_2O_4$.

Acknowledgment. We thank the Commission of the European Community (Contract No. AVI* CT92-0012), the EPSRC (for Research Grant No. GR/J76026 and providing facilities at DRAL), and the Malaysian Government (for the award of a scholarship to W.A.) for support.

CM001126Y

(72) Horvath, I.; Hanic, F. *Thermochim. Acta* **1985**, *92*, 177.

(73) Apai, G.; Monnier, J. R.; Hanrahan, M. J. *Appl. Surf. Sci.* **1984**, *19*, 307.

(74) Monnier, J. R.; Hanrahan, M. J.; Apai, G. *J. Catal.* **1985**, *92*, 119.

(75) Patniak, P.; Rao, D. Y.; Ganguli, P.; Murthy, R. S. *Thermochim. Acta* **1983**, *68*, 17.